67 Patient-Specific Eye Models for Intraocular Lens Power Calculation in Irregular Corneas

Pablo Pérez-Merino

Cataract surgery is the most common procedure performed by the ophthalmic surgeon, with more than nine million procedures executed annually worldwide. The exceptional collection of high-resolution imaging techniques to acquire precise biometric data along with the constant improvement of intraocular lens (IOL) power formulas has clearly enhanced the prediction of the refractive outcome. Although paraxial-based formulas typically offer the desired emmetropic results for patients with regular corneal surfaces and average ocular dimensions (22.5–25.5 mm of axial length), they have their own downfalls in patients with an abnormal corneal topography, such as keratoconus or eyes with previous corneal refractive surgery.

The irregular corneal surface pattern in keratoconus and the reshaping of the corneal surface after corneal refractive surgery (1) modifies the anterior-posterior corneal ratio and (2) induces significant amounts of corneal high-order aberrations (mainly, vertical coma—in keratoconus—and spherical aberration—after corneal refractive surgery). This introduces a source of error in the corneal power data input and an incorrect effective lens position (ELP) prediction for the IOL power calculation, producing a post-operative refractive surprise in most cases. Therefore, there is considerable debate about which IOL power formula and methodology match the refractive prediction in these scenarios.

The Current Landscape for IOL Power Calculation in Keratoconus

Keratoconus derives from the Greek words *Kerato* (cornea) and *Konos* (cone), and it is caused by the progressive and asymmetric weakening of the corneal tissue, in which gradual thinning lead to a cone-like appearance of the cornea, manifesting irregular astigmatism, myopia, and high levels of high-order aberrations. Symptoms of keratoconus vary and depend on its stage: from forme fruste keratoconus, with very little visual impact, to advanced stages, in which the distorted corneal surfaces severely increase astigmatism and high-order aberrations [1–7]. For these patients, cataract surgery planning presents innumerable challenges in IOL calculation due to the abnormal corneal curvature, the irregular surface pattern, an unusual anterior chamber depth, a longer axial length, and the option to combine the cataract surgery with other corneal treatments that stabilize or delay the progression of keratoconus (e.g., intracorneal ring segments [ICRS] or corneal cross-linking).

Previous studies showed that IOL power calculation in eyes with keratoconus is considerably

P. Pérez-Merino (✉)
Centre for Microsystems Technology, Ghent University and imec, Ghent, Belgium
e-mail: pablo.perezmerino@ugent.be

J. Aramberri et al. (eds.), *Intraocular Lens Calculations*, Essentials in Ophthalmology,
https://doi.org/10.1007/978-3-031-50666-6_67

Table 67.1 Refractive prediction error in eyes with three stages of keratoconus

	Mean prediction error ± standard deviation (range)		
Formula	Stage I	Stage II	Stage III
Barret	+0.63 ± 0.86 (−0.91, +2.23)	+1.32 ± 2.00 (−3.47, +5.09)	+2.64 ± 2.14 (−0.79, +6.28)
Haigis	+0.54 ± 0.79 (−0.61, +2.25)	+1.66 ± 2.05 (−2.97, +5.69)	+3.26 ± 2.38 (−0.62, +7.17)
Holladay 1	+0.75 ± 0.83 (−0.55, +2.58)	+1.54 ± 2.52 (−3.70, +3.17)	+3.77 ± 2.48 (−0.27, +7.50)
Hoffer Q	+0.90 ± 0.85 (−0.59, +2.47)	+1.63 ± 2.17 (−2.97, +6.23)	+3.46 ± 2.29 (−0.38, +6.78)
SRK/T	+0.44 ± 0.79 (−0.55, +2.32)	+0.54 ± 2.40 (−4.40, +6.09)	+3.01 ± 2.97 (−1.35, +7.17)

less accurate than for patients with regular corneal surfaces and average ocular dimensions [8–13]. In two recent publications comprising a sufficient number of series of eyes, Kamiya et al. [12] and Savini et al. [13] compared the accuracy of different conventional IOL formulas: Barret Universal 2, Haigis, Holladay 1, Hoffer Q, and SRK/T. Both studies reported that the tested formulas resulted in a hyperopic refractive outcome and found that the SRK/T was the most accurate formula with 36% and 43.9% of eyes within 0.5 diopters (D) of the final predicted refraction, respectively. However, these outcomes were much lower than that reported for normal eyes (with 75% [14] and 83% [15] of eyes within 0.5 D) and worsened noticeably in advanced stages of the disease, as we can observe in Table 67.1 (reproduced from Savini et al. [13]).

The SRK/T formula showed the highest accuracy for refractive prediction error in early and moderate stages compared with the other conventional IOL formulas; however, the post-operative refractive error was manifestly unpredictable in advanced stages for all the analyzed approaches. Melles et al. [14] described a tendency of the SRK/T formula towards myopic prediction errors with higher corneal powers in non-keratoconus eyes. This phenomenon might counterbalance the hyperopic tendency observed in early and moderate keratoconic stages (stages I and II), where the amount of high-order aberrations is relatively low; however, the refractive prediction with the SRK/T clearly failed in eyes with a higher magnitude of corneal aberrations, as keratoconic corneas in stage III, indicating that most of the assumptions made during calculations with the formula might not be valid in eyes with keratoconus and high levels of corneal aberrations.

To improve the refractive prediction in these patients, two formulas have developed specific adjustments: Kane keratoconus [16] and Holladay 2 with keratoconus adjustment [17]. The Kane keratoconus formula focuses on reducing the influence of corneal power on ELP prediction, whereas the Holladay 2 keratoconus aims to differentiate a steep keratometry reading and a small anterior segment from a patient with keratoconus, presumably to ensure that the ELP is not too affected by the high corneal power reading. Although the Kane keratoconus formula resulted in more accurate predictions compared with the Holladay 2 with keratoconus adjustment (50%-Kane vs. 27.4%-Holladay of eyes within 0.5 D), the predictability of the formula is still lower compared with patients without keratoconus and needs further refinement for IOL power calculation in keratoconus eyes, particularly in moderate and advanced stages with high levels of corneal aberrations.

IOL Power Calculation After Keratoplasty (Penetrating or Posterior Lamellar)

As in keratoconus, post-penetrating keratoplasty and posterior lamellar keratoplasty eyes are frequently associated with high refractive errors due to regular or irregular graft astigmatism and high levels of corneal aberrations, coupled with uncertain posterior corneal values and a relevant change in the anterior to posterior corneal curvature ratio [18–20]. Therefore, high unpredictability and a hyperopic refractive surprise are expected using the traditional formulas for IOL power calculation, with the SRK/T formula showing the best refractive prediction.

Present-Day Strategies for IOL Power Calculation After Corneal Refractive Surgery

The IOL power calculation after corneal refractive surgery also represents an on-going concern for surgeons and is specially challenging because the ablation profile in laser-assisted in situ keratomileusis (LASIK) or photorefractive keratectomy (PRK) modifies the anterior corneal surface (modifying the normal anterior to posterior curvature ratio) [21], changes its asphericity (e.g., more oblate cornea in a myopic treatment) [22] and induces different amounts of corneal high-order aberrations (e.g., spherical aberration) [23, 24]. In general, there are three major sources of error for the patients who have had LASIK or PRK for the treatment of myopia or hyperopia: (1) corneal power measurement, (2) keratometric index, and (3) ELP estimation [25, 26]. Actually, the proportion of eyes within 0.5 D of the final manifest refraction calculated with traditional IOL formulas (e.g., Haigis [27], Hoffer Q [28], or SRK/T [29]) was categorically low, ranging between 8.1 and 40.3% and showing again a post-operative hyperopia as a norm [26].

Therefore, numerous calculation methods, recommendations (e.g., the American Society of Cataract and Refractive Surgery (ASCRS) IOL calculation website), and modifications in the formulas have been introduced in the last years to compensate the source of errors in surgically modified eyes with LASIK or PRK. They can be classified based on a priori knowledge: (1) pre-refractive surgery keratometry and the change in the manifest refraction (pre-refractive vs. post-refractive): for example, Feiz-Mannis [30] or corneal bypass [31]; (2) change in the manifest refraction (pre-refractive vs. post-refractive): Adjusted EffRP [32], Masket's [33] and Barret True K [34], among others; and (3) no historical clinical data: Shammas [35], Awwad [36], Potvin-Hill [37], Wang-Koch-Maloney [38], Haigis-L [39], Barret True K no history or derived methods from specific equipment (e.g., Optovue RTVue and Oculus pentacam HR) [26], among others.

The methods that use pre-refractive surgery keratometry showed the poorest outcomes, with 26–44% of eyes within 0.5 D of target and significant variability; whereas, the Barret True K demonstrated the highest performance of the methods that only require the change in the manifest refraction before and after corneal refractive surgery, with 67.4% falling within 0.5 D of the final manifest refraction. The online ASCRS calculator includes most of the no historical clinical data formulas and allows simultaneous calculation using multiple formulas [40]. For example, averaging three of the included formulas (Barret True K no history, Haigis-L, and OCT-RTVue), the ASCRS calculator showed that the proportion of eyes within 0.5 D was 65.4%. Although the Barret True K and the ASCRS website meet the standards of the British National Health Service (55–85% of eyes within 0.5 D and 1.0 D, respectively) [41], the predictability of these formulas is still lower than that of an IOL power calculation for a normal eye with regular corneas and there is real need of prospective studies with larger sample sizes ($n > 40$) [26] .

Behind the Need for Change in Odd-Corneas: Three-Dimensional Corneal Shape

Corneal power is a critical variable for IOL power calculation. The options for its estimation have progressed from keratometers to topographic methods using "correction" factors of the cornea to account for the contribution of the posterior corneal curvature. On average, the radius of the curvature has a magnitude of 7.8 mm and 6.5 mm for the anterior and posterior corneal surfaces, respectively. Assuming the cornea as a single refractive surface with the anterior corneal radius and the keratometric index (n = 1.3375), the K-reading for a 7.8 mm radius would be 43.27 D. However, although the anterior corneal surface supposes the dominant factor to corneal power, the posterior cornea also has a remarkable implication. Thus, considering the refractive index of the cornea (n = 1.376), the dioptric power of the

corneal surfaces would be 48.20 D (anterior) and −6.15 D (posterior) with a total corneal power of 42.05 D; therefore, it shows a refractive discrepancy of about 1.2 D with the value obtained from the common keratometer index .

In addition, these average values (7.8 mm and 6.5 mm for the anterior and posterior corneal surfaces, respectively) show a ratio between surfaces of approximately 1.2. But, this ratio is not constant along the corneal radius range of an average eye with regular surfaces (7.5–8.0 mm: anterior surface; 5.9–6.7 mm: posterior surface) and can vary between 1.11 and 1.35 [42]. This variability is even greater in patients with keratoconus and patients with surgically modified corneas, in which there is an abnormal curvature and an irregular corneal pattern. In most keratoconic patients, the corneal topography map is characterized by focal steepening (the cone vertex is typically displaced toward the lower mid-peripheral region), and there is usually a vertical asymmetry with a certain diagonal angle, resulting in irregular astigmatism and a high magnitude of high-order aberrations (in particular, vertical coma) [1, 2, 6, 7, 43]. While the ablation profile in standard refractive surgery modifies the topographic pattern and induces a shift in the anterior corneal asphericity, toward more positive values after myopic ablation and more negative values after hyperopic ablation and the consequence of higher corneal spherical aberration (increased positive spherical aberration, in myopia correction; increased negative spherical aberration, in hyperopia correction) [22–24, 44, 45]. Figure 67.1 shows an illustration of the anterior and posterior surface pattern for a normal cornea with astigmatism, a post-LASIK cornea and a keratoconic cornea .

There is evidence that the topography pattern (toricity, asphericity, and irregularities; i.e., astigmatism, spherical aberration, and non-rotationally symmetric high-order aberrations) of both corneal surfaces, anterior and posterior, influences the refractive outcomes in the IOL power calculation [43–47]. Therefore, it is expected that the customization for the exact IOL power in all these scenarios could benefit from the inclusion of the anterior and posterior elevation corneal data in the calculation methods, instead of simplified corneal parameters such as the corneal power with their innumerable assumptions .

To date, there is a huge variety of commercial systems to measure corneal topography that can be classified based on the imaging principle: specular reflection, scattered light, Scheimpflug imaging, and optical coherence tomography (OCT) [48]. Scheimpflug and OCT are the only imaging techniques that generate true elevation points with micron-resolution of both corneal surfaces, anterior and posterior [3, 49–51]. Figure 67.2 shows an illustration of three-dimensional OCT corneal analysis and representation.

Assuming that the corneal surface is given by $z = f(x,y)$ in a Cartesian system with first and second derivatives continuous at any point, there are three ways of representing corneal topography [52]:

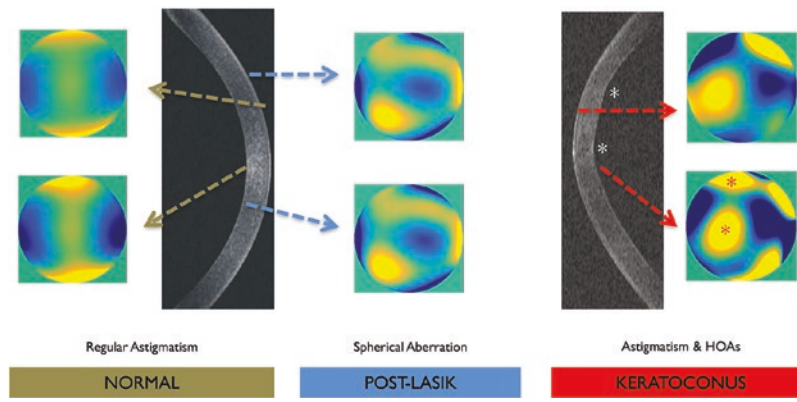

Fig. 67.1 Anterior and posterior corneal surface pattern for a normal cornea with regular astigmatism, a post-LASIK cornea with higher amounts of spherical aberration and a keratoconic cornea with irregular surfaces and higher levels of astigmatism and high-order aberrations (*denotes the different vertex locations in the posterior corneal surface)

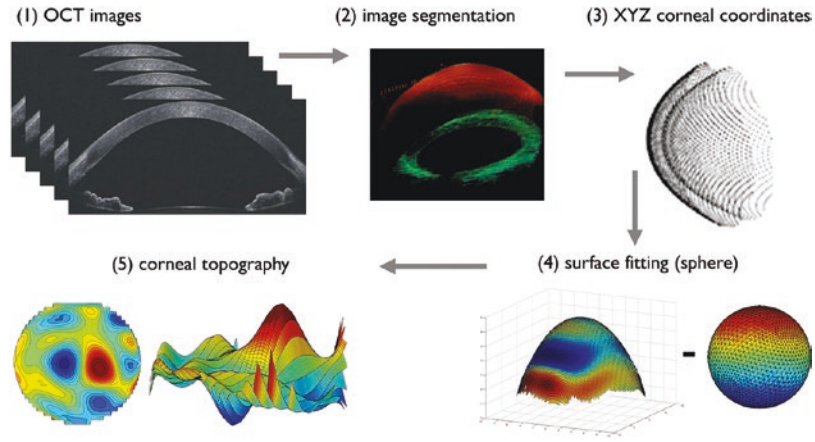

Fig. 67.2 Illustration of the OCT segmentation process and calculation of the topographic map from direct subtraction of the elevation data minus the best fitted-sphere

- By *surface elevation f(x,y)* with respect to a reference surface (e.g., sphere). A typical reference sphere is one with the minimum standard deviation with respect to the corneal surface and with the same optical axis. The best-fit sphere to evaluate the topography of the cornea is calculated using a least squares method.
- By *local slopes* with respect to the reference sphere, since at any point on the surface, the slope is a function of the direction.
- By *local curvature*, for a given point, there is a maximum value in a certain direction and a minimum value in the perpendicular direction.

The corneal surface data is commonly expressed in Euclidean coordinates, and it is fitted by standard functions: sphere (from the sphere we obtain the radius and the center of the sphere), ellipsoid (from the ellipsoid we obtain three radii of curvature and the center of the ellipsoid), conicoid (the fitting parameters of the conicoid are the radius and the conic constant), or Zernike polynomial expansions (note that these are fits to surface elevations, not corneal wave aberrations).

Patient-Specific IOL Power Calculation: Ray Tracing

Patient-specific IOL selection by virtual ray-tracing eye modeling is gaining awareness amongst IOL manufacturing companies and the ophthalmology community since this methodology:

1. Exploits the complete information of the corneal topography for IOL power calculation, considering the anterior and posterior surface pattern of the cornea (XYZ surface coordinates or Zernike polynomial expansions of the anterior and posterior surfaces) instead of simplified corneal parameters
2. Allows realistic individual simulations of defocus, astigmatism, and high-order aberrations and any associated change in retinal image quality, i.e., influence of patient's corneal topography (avoiding, for example, the keratometry error of an aspheric cornea), IOL design (monofocal, toric, and multifocal), IOL positioning (including tolerance to tilt and decentration), impact of the corneal incision, decentered pupil, and foveal misalignment

Geometric optics assumes that the wavelength of the light is sufficiently small, so light propagation can be described in terms of rays and it is calculated by applying the Snell's law. Analyzing the optical system by tracing many rays through multiple analytical surfaces is therefore known as ray tracing, and in terms of geometrical optics every deviation from a perfect optical system can be quantified as optical aberrations.

Most of the current generic eye modeling requires the assistance of ray tracing computational programs, optical optimization by integrating a merit function in order to approach the specific targets (e.g., best focal position and optical quality metrics) and the definition of different

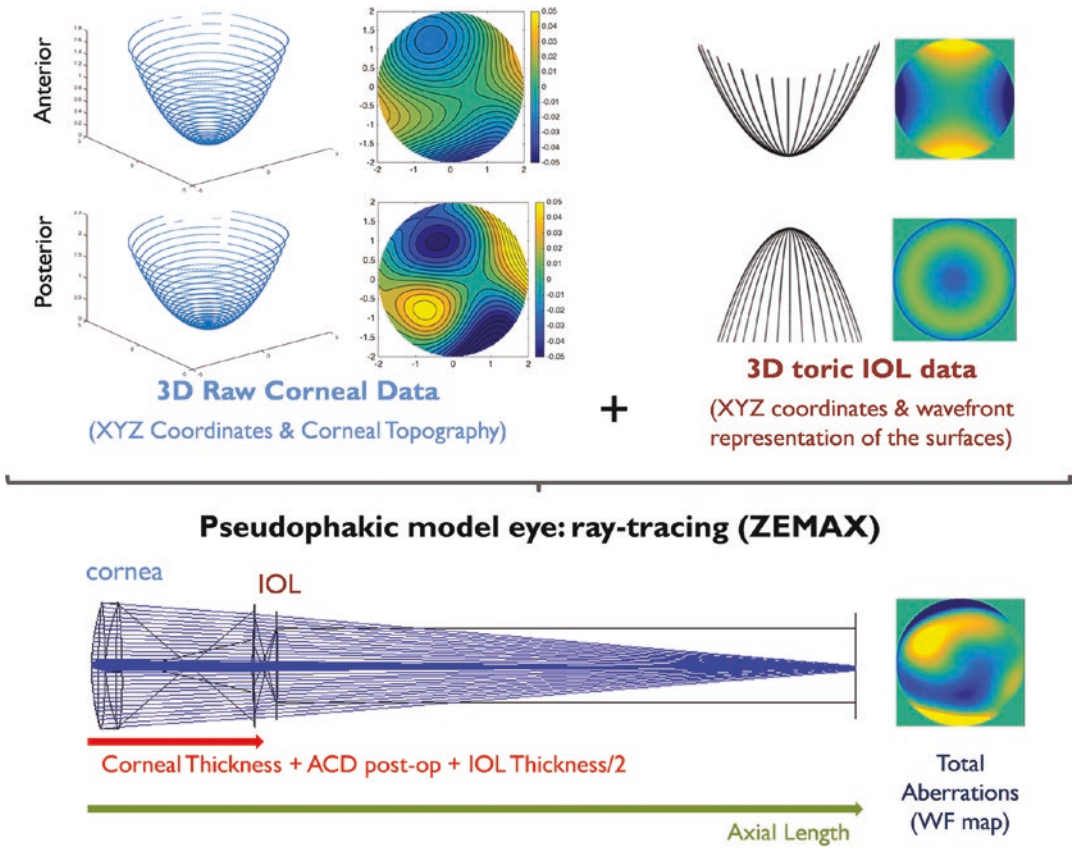

Fig. 67.3 Ray-tracing personalized eye model in ZEMAX. Three-dimensional corneal (Sirius, CSO, Firenze, Italy) and IOL data (Precizon Toric, OPHTEC BV, Groningen, The Netherlands)

variables: (1) position of the object point, (2) position and shape of the image surface (normally a plane), (3) stop surface and diameter, which defines the entrance-exit pupil size and position, and (4) wavelength. The most common programs to generate ray-tracing eye models are as follows: ZEMAX (Radiant ZEMAX; Focus software, Tucson, AZ), Code V (Optical Research Associates, Pasadena, CA), ASAP (Breault Research Organization, Inc., Tucson, AZ) and OSLO (Lambda Research Corporation, Littleton, MA) [46, 53–62]. Furthermore, examples of ray tracing modules for IOL power calculation found on commercially available corneal topographers are Olsen's PhacoOptics (IOL Innovations ApS, Aarhus, Denmark) and Okulix (Okulix, Dortmund, Germany). In these modules, following determination of the anterior and posterior corneal surfaces, thicknesses and refractive indices, the IOL is modelled to determine the effective focal length that matches the axial length, i.e., the IOL power and cylinder is calculated to minimize the refractive error (with zero defocus and astigmatism as the final refractive target) [63]. Figure 67.3 illustrates the computation of ocular aberrations in the pseudophakic eye model using ZEMAX.

One key issue is the ELP, a very sensitive variable in IOL selection and also challenging to precisely estimate from the data of pre-operative measurements [64]. Most of paraxial-based IOL power formulas typically correlated the ELP with one or more pre-surgery biometry measurements, including anterior chamber depth (ACD), anterior corneal curvature, and axial length. However, these parameters are unrelated to the crystalline lens, and therefore, some uncertainty in the prediction is expected, since the IOL position will depend on the individual shrinkage of the capsular bag.

Recent improvements in biometry imaging techniques and image processing tools for accurate three-dimensional quantification of the anterior segment, especially with OCT technology in the spectral domain configuration, have opened the possibility of considering different crystalline lens variables [65–68]. Latest ELP approaches included three-dimensional crystalline lens parameters (lens volume, surface area, diameter, and equatorial plane position) and found in the pre- and post-operative measurements a strong correlation between the geometry of the crystalline lens and the IOL position [69]. Therefore, it would be possible to create patient-specific eye models (i.e., anterior and posterior corneal topography, accurate axial distances, IOL nominal values, and ray tracing) that include an accurate ELP based on the pre-operative shape of the crystalline lens.

Redefining the Refractive Target: Matching the Ideal IOL in Keratoconus and Surgically Modified Patients

To date, IOL power calculation methodologies, including ray tracing, estimate the IOL power by minimizing the refractive error, with zero defocus and astigmatism as the optimum post-operative target in all the scenarios. However, it has been demonstrated that the optical quality could be improved by adding certain amounts of spherical aberration to a given level of defocus, as well as specific amounts of astigmatism and coma can interact favourably to increase the visual performance (Fig. 67.4) [70–72]. As a consequence, the contribution of spherical aberration, coma, and other high-order aberrations to the target refraction needs to be considered.

Therefore, a specific magnitude of defocus and astigmatism in combination with the natural corneal high-order aberrations might improve the visual performance and enhance the prediction of the refractive outcome. Under this premise, the online calculator *https://www.exactiol.com* proposes a novel methodology for a patient-specific IOL selection based on exact ray tracing, simulated visual performance at different light conditions and through-focus optimization. The program uses the anterior and posterior corneal elevation maps and artificial neural networks to accurately calculate the IOL power and cylinder.

The results of the exactiol calculator in different group of patients are shown in the following figures (Figs. 67.5, 67.6, 67.7, and 67.8). Figure 67.5 illustrates the simulated visual performance (Snellen E letter) of a patient with keratoconus (Fig. 67.5a) and two post-LASIK patients (Fig. 67.5b, myopic-LASIK; Fig. 67.5c, hyperopic-LASIK). This figure shows the visual performance for a 4-mm pupil diameter in (1) the pre-operative condition with the values of astigmatism, spherical and high-order aberrations of the cornea: −4.5D at 85 degrees of astigmatism, −0.24 μm of spherical aberrations and the root mean square of high-order aberrations (RMS HOAs) of 0.53 μm (keratoconus); −1.00D at 120 degrees of astigmatism, +0.20 μm of spherical aberrations and the RMS HOAs of 0.42 μm (post-LASIK myopia); −0.75D at 120 degrees of astigmatism, −0.05 μm of spherical aberrations and the RMS HOAs of 0.28 μm (post-LASIK hyperopia). (2) Zero defocus and astigmatism in combination with the natural corneal aberrations. (3) The ideal defocus and astigmatism for this amount of high-order corneal aberrations: +1.5D −0.75D at 125° (keratoconus); −1.25D −0.75D at 180° (post-LASIK myopia); +0.25D −0.50 D at 160 degrees (post-LASIK hyperopia). As we can see, there is an ideal combination of defocus and astigmatism that produces the highest visual performance.

Specifically, plotting the through-focus curve in the representative keratoconus example (Fig. 67.6), we appreciate the visual benefit of the optimization process in which a certain magnitude of defocus and astigmatism lead to an increase in peak Visual Strehl values. For this example, the comparison of the traditional formula SRK/T vs. exactiol showed a difference in power and cylinder in the final IOL calculation of 1D, in power, and 1D −5°, in cylinder (SRK/T: Power: 14D; cylinder: 5.5D at 85°. Exactiol: Power: 13D; cylinder: 6.5D at 80°).

In Fig. 67.7, we can see how eyes with low visual quality have most to gain in terms of visual

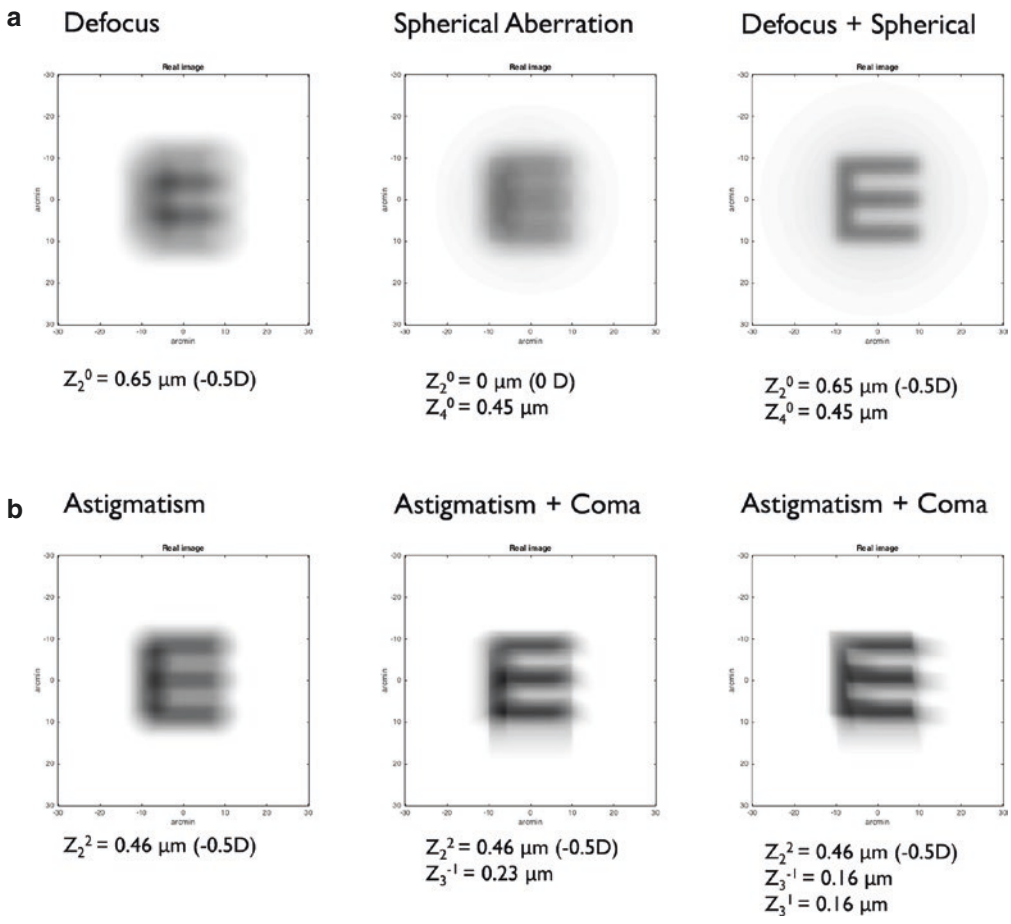

Fig. 67.4 Simulated visual acuity of the Snellen E-letter of 20 arc-min for 6-mm pupil diameter. (**a**) −0.5 D of defocus—left panel; +0.45 microns of spherical aberration—center panel; −0.5 D of defocus with +0.45 microns of spherical aberration—right panel. (**b**): −0.5 D of astigmatism at 0°—left panel; −0.5 D of astigmatism at 0° with 0.23 microns of coma at 45°—center panel; −0.5 D of astigmatism at 0° with 0.23 microns of coma at 90°—right panel (reproduced from de Gracia et al. [72])

benefit, that means, corneas with higher levels of corneal aberrations presented greater visual improvement with an optimized refractive target. On average, the ideal post-operative astigmatism target would be around 1 D for a cornea with a RMS HOAs of 0.3 microns, while the astigmatism target would be around 2 D for a cornea with a RMS HOAs of 0.6 microns (this analysis included 184 irregular corneas; pupil diameter: 4-mm).

Finally, Fig. 67.8 plots the post-operative defocus target as a function of the pre-operative spherical aberration (left) and as a function of spherical aberration, astigmatism, and high-order aberrations (right). As expected, in addition to the amount of spherical aberration (i.e., asphericity), the levels of corneal astigmatism and high-order aberrations have a manifest impact in the final IOL power calculation, offering us a unique opportunity for an accurate IOL selection.

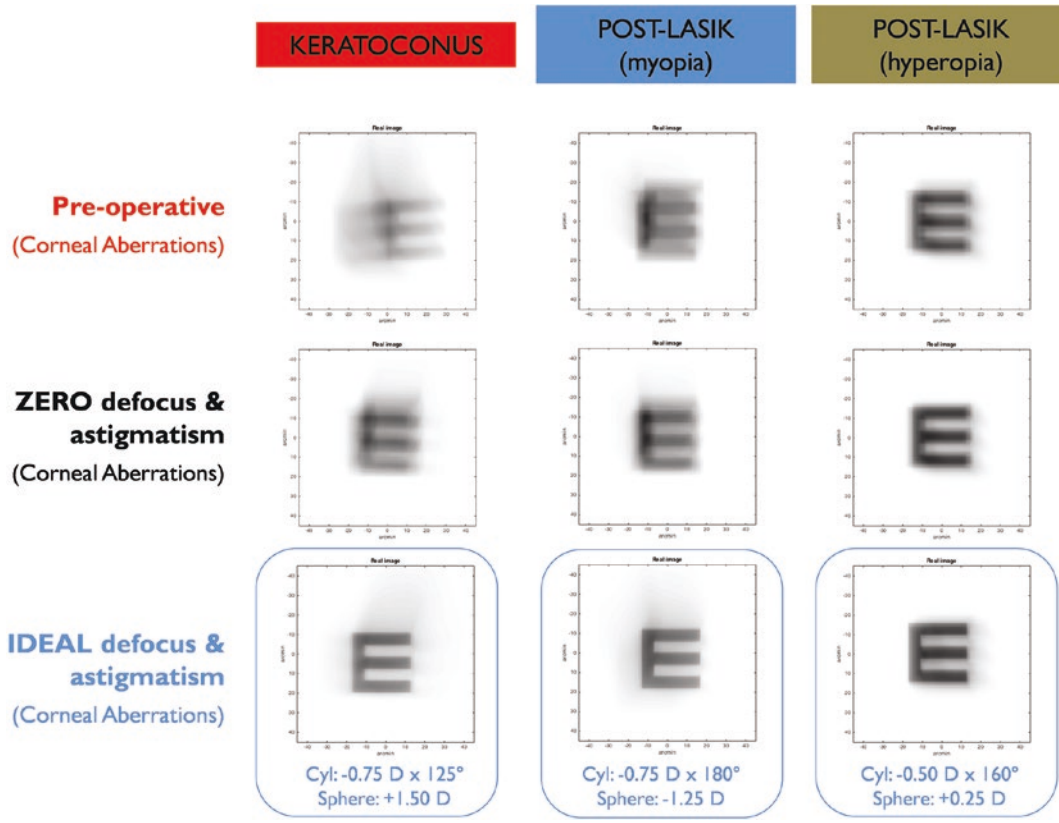

Fig. 67.5 Theoretical simulations of the Snellen E-letter of 30 arc-min for 4-mm pupil diameter in different patients with odd-corneas: keratoconus and surgically modified (post-LASIK myopia and post-LASIK hyperopia). Top: convolved letter with the pre-operative amount of astigmatism and high-order aberrations. Center: convolved letter with the natural corneal high-order aberrations (cancelling defocus and astigmatism). Bottom: convolved letter with the natural corneal high-order aberrations and the amount of defocus and astigmatism that produced the best optical quality

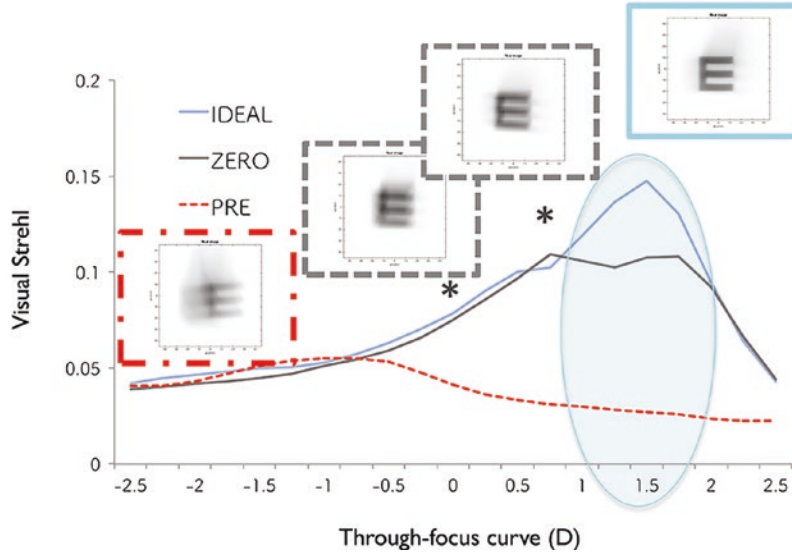

Fig. 67.6 Through-focus Visual Strehl for the keratonic eye and the corresponding convolved images: pre-operative (red), zero astigmatism (grey), and 0.75 D of astigmatism at 125° (light blue)

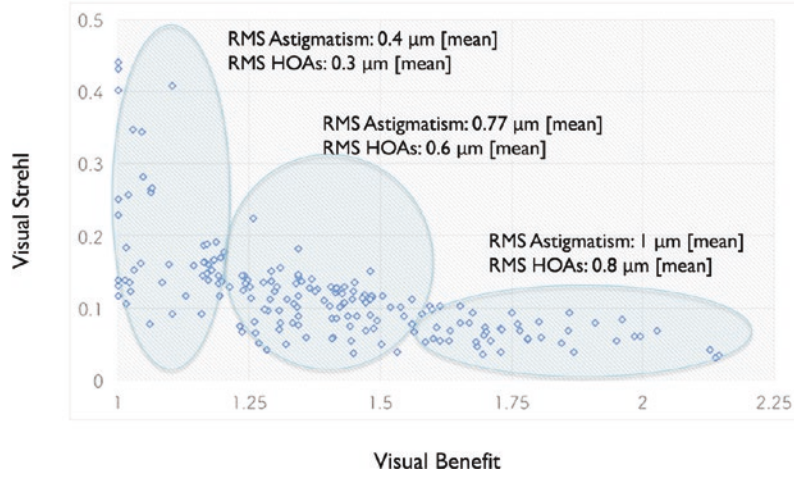

Fig. 67.7 Visual benefit of considering the natural corneal aberrations and astigmatism for the IOL power calculation

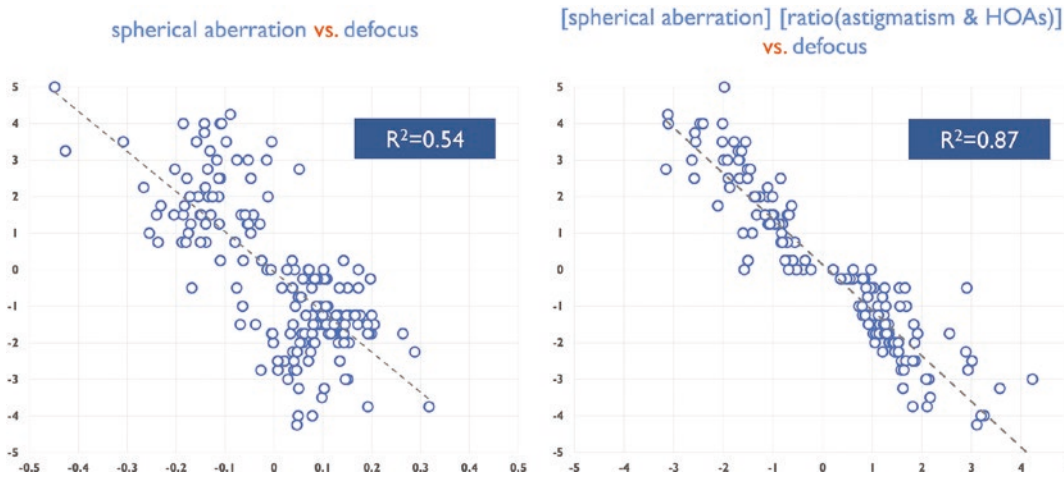

Fig. 67.8 IOL power prediction as a function of the corneal astigmatism and high-order aberrations. Left: Defocus vs. Spherical aberration. Right: Defocus vs. Spherical aberration, astigmatism, and HOAs

Personalized Surgical Planning

Another area of discussion in these patients is the selection of the IOL type: monofocal vs. toric vs. multifocal. Toric IOL implantation has been shown to be a feasible option for patients with non-progressive forme fruste or moderate keratoconus. However, different studies showed that the post-operative refractive astigmatism after a toric IOL implantation differed from the planned target of zero astigmatism from 0.8 to 6.9 D using the traditional formulas [10, 12, 73]. Besides, a key issue is the tolerance to decentration and rotational stability of the toric design, since decentration and/or rotation results in an induction of astigmatism and coma [74]. Regarding the IOL selection in post-LASIK eyes, state-of-the-art monofocal IOLs have aspheric surfaces with the aim at reducing the positive spherical aberration of the average cornea, mimicking the spherical aberration balance between the cornea and crystalline lens in the young eye. However, some caution is needed with the aspheric IOL design and the spherical aberration compensation, since patients who had myopic LASIK/PRK had increased positive spherical aberration values, whereas those who had hyperopic LASIK/PRK had increased the magnitude of negative corneal spherical aberration [45]. Moreover, in these

groups of patients, a contraindication for the implantation of a multifocal IOL is the level of high-order aberrations; but, to date, there are no guidelines about the cut-off values of corneal aberrations in the implantation of multifocal IOLs. So, there is a critical window of opportunity to harness IOL selection and surgical planning with patient-specific eye models:

1. Cataract surgery tends to render defocus and astigmatism neutral but minimizing the refractive error (with zero defocus and astigmatism as the final refractive target) is not the best strategy for keratoconus and surgically modified corneas, since the position of best focus is highly influenced by the presence of corneal astigmatism and high-order aberrations.
2. Centration and rotational stability is more critical with the increasing complexity of toric and multifocal IOL designs; thus, it is essential to incorporate the three-dimensional IOL design to evaluate the simulated visual performance and tolerance to decentration and multifocality of a specific cornea. With the incorporation of the three-dimensional corneal geometry and the IOL design in the eye models, it would possibly design a customized strategy to define the cut-off values of astigmatism and high-order aberrations in the implantation of toric and multifocal IOLs.
3. Even with small corneal incisions and fixed meridians, not only surgically induced astigmatism (SIA) is highly variably but also there is lack of evidence about the surgically induced coma (SIC) and/or trefoil (SIT). The three-dimensional analysis of the corneal surfaces and different refractive corneal parameters (i.e., power vectors of astigmatism, coma and trefoil) might open new avenues to predict the impact of the surgical induced changes in the corneal surfaces.

$$\text{Pupil function } g\left(x',y'\right) = p\left(x',y'\right)\exp\left(i\frac{2\pi}{\lambda}W\left(x,y\right)\right) \tag{67.1}$$

where *p(x',y')* is a circle that defines the aperture of the eye, *w(x',y')* is the wavefront aberration of the subject and λ the wavelength used for calculations (550 nm).

$$\text{PSF} = \left|FT\left(g\left(x',y'\right)\right)\right|^2 \tag{67.2}$$

$$\text{OTF} = FT\left(PSF\right) \tag{67.3}$$

$$\text{MTF} \# OTF \# \tag{67.4}$$

$$\text{Strehl Ratio} = \frac{PSF_{\text{aberrated}}\left(x',y'\right)}{PSF_{\text{ideal}}\left(x',y'\right)} \tag{67.5}$$

$$\text{CSF} = MTF_{\text{optical}} * MTF_{\text{neural}} \tag{67.6}$$

$$\text{VSOTF} = \frac{\int_{-\infty}^{\infty}\int_{-\infty}^{\infty}\text{CSF}_N\left(f_x,f_y\right)\#\ \text{Re}\left\{\text{OTF}\left(f_x,f_y\right)\right\}\#\ df_x df_y}{\int_{-\infty}^{\infty}\int_{-\infty}^{\infty}\text{CSF}_N\left(f_x,f_y\right) * \left\{\text{OTF}\left(f_x,f_y\right)\right\} df_x df_y} \tag{67.7}$$

where $\text{OTF}(f_x f_y)$ denotes the diffraction-limited OTF, $\text{CSF}_N(f_x f_y)$ is the neural contrast sensitivity function, and $(f_x f_y)$ are the spatial frequency coordinates. Here, the VSOTF was based on calculated OTF across all spatial frequencies.

Appendix 1 Patient-Specific Ray-Tracing Eye Model (ZEMAX)

The commercial software of most corneal topographers allows the extraction of the raw elevation

points of the anterior and posterior corneal surfaces and corneal thickness. For example, in Pentacam (OCULUS Optikgeräte GmbH, Wetzlar, Germany): the [Export] button in the Patient Data Management exports the chosen examinations directly to the folder Pentacam.exp (PatientID_Eye_Date_Hour.ELE and PatientID_Eye_Date_Hour.PAC; .ELE and .PAC contains the XYZ coordinates of the surfaces), while in Sirius and MS39 (CSO, Firenze, Italy): the Phoenix v2.1 software from CSO permits to export the following data from the tomographer: PatientID.csv and PatientID.xyX). The Pentacam raw data consists of the elevation value for every corneal point sampled in a Cartesian grid (from −7 to +7 mm, nasal-temporal, superior-inferior) in 100 μm steps. The Sirius and MS-39 raw data comprises 7937 anterior and posterior elevation points over a polar grid with 256 meridians (from −6 to +6 mm, nasal-temporal, superior-inferior).

One key issue is to convert the data format used by the instrument into a suitable structure for the ray-tracing in ZEMAX. For example, the corneal elevation data file could be fitted with Zernike polynomial expansions and imported into ZEMAX using the *Zernike sag surface* type (note that *Zernike sag surface* in ZEMAX is in Noll's format; hence, previous conversion is needed since Noll's notation differs from the OSA standards).

Regarding the IOL, a *standard* ZEMAX surface type (radius, asphericity, thickness, and refractive index) is acceptable to calculate the ocular aberrations (cornea and IOL) and predict the refractive error of a monofocal IOL. Although the *Zernike sag surface* could be also used if the three-dimensional design of the IOL is available.

For ray-tracing in ZEMAX, the object (light source) is set at infinity. The point source at infinity will be best focused on the retinal surface after iteration (for example, the best focus position as is the position that minimizes the root-mean-square wavefront error). Refractive indices of 1.376 and 1.336 are commonly used for the cornea and aqueous humor, respectively. Wave aberrations for the defined pupil diameter (e.g., 4-mm pupil diameter) are calculated for the defined wavelenght (e.g., monochromatic light at 555 nm), by tracing an array of 64 × 64 rays collimated through a 2-surface model (anterior and posterior cornea, separated by corneal thickness) and 4-surface model (adding to the corneal surfaces: the nominal values of the IOL, the estimated lens position (e.g., anterior chamber depth post-op+IOL thickness/2), and the axial length. Pseudophakic eyes are simpler than phakic eye models to analyze the optical quality, as the refractive index of the IOL is constant and the surfaces curvature are known.

The optical performance of the pseudophakic eye model is evaluated with the three-dimensional representation (*3D Layout*), the *Spot Diagram,* and the Zernike wavefront aberrations (*Zernike Standard Coefficients*). Figure 67.3 shows an illustration of a personalized eye model in ZEMAX using three-dimensional corneal and IOL data.

Appendix 2 Optical Aberrations and Image Quality Metrics

The image-forming properties of any optical system can be described in terms of wave aberration. Light can be considered as a series of waves coming from a source. In aberrations-free optical systems, all the parallel rays will intersect the retina at the same point, or equivalently, all the imaging wavefronts will be spherical and centered in the image point. However, an imperfect lens will impose phase distortions on the plane waves, there is no longer a focal point and the different rays will intersect the image plane at different points (the wavefronts will no longer be spherical). The difference between the distorted waves and the ideal waves is the wavefront aberration, representing the distortions of the wavefront (surface containing points with the same phase and orthogonal to the propagation axis) in the pupil plane as it goes through the optical system.

The *wave aberration* of a general optical system can be described mathematically by a polynomial series. Zernike polynomial expansion has become the standard for representing wave aberration data because they form an orthogonal set over a circle of unit radius, and aberrations are usually referred to circular pupils. An interesting

feature of the Zernike polynomials is that some terms are directly related to commonly known ocular aberrations. For example, structural abnormalities of the eye, such as myopia, hyperopia and astigmatism, appear in the second order of this expansion. Further, Zernike terms represent higher-order aberrations such as spherical aberration (arising from the asphericity of the optical surfaces) and coma (mainly associated to local irregularities, tilt, and decentration of the surfaces of the optical system).

From the wave aberration coefficients, different optical quality descriptors can be directly derived after mathematical operations [71, 75–80]. The two classic descriptors are the *Modulation Transfer Function (MTF)* and the *Point Spread Function (PSF)*. The MTF quantifies the loss in contrast associated to each spatial frequency, the higher the MTF, the better the image provided by the system. The PSF is the impulse response of the system, i.e., the degraded image of an ideal point as imaged by the system. The PSF is calculated as the squared magnitude of the inverse Fourier transform of the pupil function (the pupil function defines how light passes through the pupil). The *Root Mean Square (RMS)* is also a common descriptor; it is defined as the root square of the variance of the wave aberration and is typically used as the global metric for the optical quality. The *Strehl ratio* is a scalar metric used to describe the quality of the PSF in an eye. As the Strehl ratio includes in the calculation regions of the MTF with spatial frequencies beyond those relevant to the visual system, a new metric is introduced to adapt the definition to visual optics (Visual Strehl). The *Visual Strehl* has been shown to hold the highest correlation variance against subjective acuity. It is computed as the volume under the visual MTF, obtained from the overlapping of the MTF with the inverse of a general neural transfer function, normalized to diffraction limit. The neural sensitivity, function of the spatial frequency, is a common measurement of the neural performance. In a similar way as the optical MTF, it is possible to define and measure the neural MTF, and the product of the neural and optical MTFs gives the Contrast Sensitivity Function (CSF) of the eye.

References

1. Nordan LT. Keratoconus: diagnosis and treatment. Int Ophthalmol Clin. 1997;37(1):51–63.
2. Rabinowitz YS. Keratoconus. Surv Ophthalmol. 1998;42(4):297–319.
3. Tomidokoro A, Oshika T, Amano S, et al. Changes in anterior and posterior corneal curvatures in keratoconus. Ophthalmology. 2000;107(7):1328–32.
4. Saad A, Gatinel D. Topographic and tomographic properties of forme frustre keratoconus corneas. Invest Ophthalmol Vis Sci. 2010;51(11):5546–55.
5. Alio JL, Shabayek MH. Corneal higher order aberrations: a method to grade keratoconus. J Refract Surg. 2006;22(6):539–45.
6. Barbero S, Marcos S, Merayo-Lloves J, et al. Validation of the estimation of corneal aberrations from videokeratography in keratoconus. J Refract Surg. 2002;18:263–70.
7. Maeda N, Fujikado T, Kuroda T, et al. Wavefront aberrations measured with Hartmann-Shack sensor in patients with keratoconus. Ophthalmology. 2002;109(11):1996–2003.
8. Navas A, Suárez R. One-year follow-up of toric intraocular lens implantation in forme fruste keratoconus. J Cataract Refract Surg. 2009;35:2024–7.
9. Nanavaty MA, Lake DB, Daya SM. Outcomes of pseudophakic toric intraocular lens implantation in keratoconic eyes with cataract. J Refract Surg. 2012;28:884–9.
10. Hashemi H, Heidarian S, Seyedian MA, Yekta A, Khabazkhoob M. Evaluation of the results of using toric IOL in the cataract surgery of keratoconus patients. Eye Contact Lens. 2015;41:354–8.
11. Kamiya K, Shimizu K, Miyake T. Changes in astigmatism and corneal higher-order aberrations after phacoemulsification with toric intraocular lens implantation for mild keratoconus with cataract. Jpn J Ophthalmol. 2016;60:302–8.
12. Kamiya K, Iijima K, Nobuyuki S, Mori Y, Miyata K, Yamaguchi T, Shimazaki J, Watanabe S, Maeda N. Predictability of intraocular lens power calculation for cataract with keratoconus: a multicenter study. Sci Rep. 2018;8(1):1312.
13. Savini G, Abbate R, Hoffer KJ, Mularoni A, Imburgia A, Avoni L, D'Eliseo D, Schiano-Lomoriello D. Intraocular lens power calculation in eyes with keratoconus. J Cataract Refract Surg. 2019;45(5):576–81.
14. Melles RB, Holladay JT, Chang WJ. Accuracy of intraocular lens calculation formulas. Ophthalmology. 2018;125:169–78.
15. Melles RB, Kane JX, Olsen T, Chang WJ. Update on intraocular lens calculation formulas. Ophthalmology. 2019;126:1334–5.
16. Kane JX, Connell B, Yip H, McAlister JC, Beckingsale P, Snibson GR, Chan E. Accuracy of intraocular lens power formulas modified for patients with keratoconus. Ophthalmology. 2020;127(8):1037–42.

17. Holladay JT. Holladay IOL Consultant software and surgical outcomes assessment. 1105.2019 ed. Bellaire: Holladay Consulting; 2019.
18. Koch DD. The enigmatic cornea and intraocular lens calculations: the LXXIII Edward Jackson memorial lecture. Am J Ophthalmol. 2016;171:xv–xxx.
19. Lockington D, Wang EF, Patel DV, Moore SP, McGhee CN. Effectiveness of cataract phacoemulsification with toric intraocular lenses in addressing astigmatism after keratoplasty. J Cataract Refract Surg. 2014;40(12):2044–9.
20. Wade M, Steinert RF, Garg S, Farid M, Gaster R. Results of toric intraocular lenses for post-penetrating keratoplasty astigmatism. Ophthalmology. 2014;121(3):771–7.
21. Aramberri J. Intraocular lens power calculation after corneal refractive surgery: double-K method. J Cataract Refract Surg. 2003;29(11):2063–8.
22. Anera RG, Jiménez JR, Jiménez del Barco L, Bermudez J, Hita H. Changes in corneal asphericity after laser in situ keratomileusis. J Cataract Refract Surg. 2003;29(4):762–8.
23. Marcos S, Barbero S, Llorente L, Merayo-Lloves J. Optical response to LASIK surgery for myopia from total and corneal aberration measurements. Invest Ophthalmol Vis Sci. 2001;42(13):3349–56.
24. Moreno-Barriuso E, Lloves JM, Marcos S, Navarro R, Llorente L, Barbero S. Ocular aberrations before and after myopic corneal refractive surgery: LASIK-induced changes measured with laser ray tracing. Invest Ophthalmol Vis Sci. 2001;42(6):1396–403.
25. Hoffer KF. Intraocular lens power calculation after previous laser refractive surgery. J Cataract Refract Surg. 2009;35(4):759–65.
26. Pantanelli SM, Lin CC, Al-Mohtaseb Z, Rose-Nussbaumer JR, Santhiago MR, Steigleman WA 3rd, Schallhorn JM. Intraocular lens power calculation in eyes with previous excimer laser surgery for myopia: a report by the American Academy of Ophthalmology. Ophthalmology. 2021;128(5):781–92.
27. Haigis W, Lege B, Miller N, Schneider B. Comparison of immersion ultrasound biometry and partial coherence interferometry for intraocular lens calculation according to Haigis. Graefes Arch Clin Exp Ophthalmol. 2000;238(9):765–73.
28. Hoffer KJ. The Hoffer Q formula: a comparison of theoretic and regression formulas. J Cataract Refract Surg. 1993;19(6):700–12.
29. Retzlaff JA, Sanders DR, Kraff MC. Development of the SRK/T intraocular lens implant power calculation formula. J Cataract Refract Surg. 1990;16(3):333–40.
30. Feiz V, Mannis MJ, Garcia-Ferrer F, Kandavel G, Darlington JK, Kim E, Caspar J, Wang JL, Wang W. Intraocular lens power calculation after laser in situ keratomileusis for myopia and hyperopia: a standardized approach. Cornea. 2001;20(8):792–7.
31. Walter KA, Gagnon MR, Hoopes PC Jr, Dickinson PJ. Accurate intraocular lens power calculation after myopic laser in situ keratomileusis, bypassing corneal power. J Cataract Refract Surg. 2006;32(3):425–9.
32. Hamed AM, Wang L, Misra M, Koch DD. A comparative analysis of five methods of determining corneal refractive power in eyes that have undergone myopic laser in situ keratomileusis. Ophthalmology. 2002;109(4):651–8.
33. Masket S, Masket SE. Simple regression formula for intraocular lens power adjustment in eyes requiring cataract surgery after excimer laser photoablation. J Cataract Refract Surg. 2006;32(3):430–4.
34. Abulafia A, Hill WE, Koch DD, Wang L, Barrett GD. Accuracy of the Barrett True-K formula for intraocular lens power prediction after laser in situ keratomileusis or photorefractive keratectomy for myopia. J Cataract Refract Surg. 2016;42(3):363–9.
35. Shammas HJ, Shammas MC. No-history method of intraocular lens power calculation for cataract surgery after myopic laser in situ keratomileusis. J Cataract Refract Surg. 2007;33(1):31–6.
36. Awwad ST, Manasseh C, Bowman RW, Cavanagh HD, Verity S, Mootha V, McCulley JP. Intraocular lens power calculation after myopic laser in situ keratomileusis: estimating the corneal refractive power. J Cataract Refract Surg. 2008;34(7):1070–6.
37. Potvin R, Hill W. New algorithm for intraocular lens power calculations after myopic laser in situ keratomileusis based on rotating Scheimpflug camera data. J Cataract Refract Surg. 2015;41(2):339–47.
38. Wang L, Hill WE, Koch DD. Evaluation of IOL power prediction methods using the ASCRS post-keratorefractive IOL power calculator. J Cataract Refract Surg. 2010;36:1466–73.
39. Haigis W. Intraocular lens calculation after refractive surgery for myopia: Haigis-L formula. J Cataract Refract Surg. 2008;34:1658–63.
40. Hill W, Wang L, Koch DD. IOL power calculation in eyes that have undergone LASIK/PRK/RK. https://iolcalc.ascrs.org.
41. Gale RP, Saldana M, Johnston RL, Zuberbuhler B, McKibbin M. Benchmark standards for refractive outcomes after NHS cataract surgery. Eye. 2009;23:149–52.
42. Olsen T. Calculation of intraocular lens power: a review. Acta Ophthalmol Scand. 2007;85(5):472–85.
43. Goto S, Maeda N. Corneal topography for intraocular lens selection in refractive cataract surgery. Ophthalmology. 2021;128:e142–52. S0161-6420(20)31108-1108.
44. Holladay JT. Effect of corneal asphericity and spherical aberration on intraocular lens power calculations. J Cataract Refract Surg. 2015;41(7):1553–4.
45. Canovas C, Abenza S, Alcon E, Villegas EA, Marin JM, Artal P. Effect of corneal aberrations on intraocular lens power calculations. J Cataract Refract Surg. 2012;38(8):1325–32.
46. Canovas C, Artal P. Customized eye models for determining optimized intraocular lenses power. Biomed Opt Express. 2011;2(6):1649–62.
47. Wang L, Koch DD. Intraocular lens power calculations in eyes with previous corneal refractive sur-

gery: review and expert opinion. Ophthalmology. 2021;128(11):e121–31. S0161-6420(20)30625-4.
48. Mejia-Barbosa Y, Malacara-Hernandez D. A review of methods for measuring corneal topography. Optom Vis Sci. 2001;78:240–53.
49. Ortiz S, Siedlecki D, Perez-Merino P, Chia N, de Castro A, Szkulmowski M, Wojtkowski M, Marcos S. Corneal topography from spectral optical coherence tomography (sOCT). Biomed Opt Express. 2011;2:3232–47.
50. Pérez-Merino P, Ortiz S, Alejandre N, de Castro A, Jimenez-Alfaro I, Marcos S. Ocular and optical coherence tomography-based corneal aberrometry in keratoconic eyes treated by intracorneal ring segments. Am J Ophthalmol. 2014;157:116–27.
51. Pérez-Merino P, Ortiz S, Alejandre N, Jimenez-Alfaro I, Marcos S. Quantitative OCT-based longitudinal evaluation of intracorneal ring segment implantation in keratoconus. Invest Ophthalmol Vis Sci. 2013;54:6040–51.
52. Sicam V, Van der Heijde RGL. Topographer reconstruction of the nonrotation-symmetric anterior corneal surface features. Optom Vis Sci. 2006;83(12):910–8.
53. Zhu Z, Janunts E, Eppig T, Sauer T, Langenbucher A. Tomography-based customized IOL calculation model. Curr Eye Res. 2011;36(6):579–89.
54. Preussner PR, Wahl J, Lahdo H, Dick B, Findl O. Ray tracing for intraocular lens calculation. J Cataract Refract Surg. 2002;28(8):1412–9.
55. Preussner PR, Wahl J, Weitzel D. Topography-based intraocular lens power selection. J Cataract Refract Surg. 2005;31(3):525–33.
56. Preussner PR, Olsen T, Hoffmann P, Findl O. Intraocular lens calculation accuracy limits in normal eyes. J Cataract Refract Surg. 2008;34(5):802–8.
57. Hoffmann P, Wahl J, Preussner PR. Accuracy of intraocular lens calculation with ray tracing. J Refract Surg. 2012;28(9):650–5.
58. Olsen T, Hoffmann P. C constant: new concept for ray tracing-assisted intraocular lens power calculation. J Cataract Refract Surg. 2014;40(5):764–73.
59. Hoffmann PC, Wahl J, Hütz WW, Preußner PR. A ray tracing approach to calculate toric intraocular lenses. J Refract Surg. 2013;29(6):402–8.
60. Sun M, Pérez-Merino P, Martinez-Enriquez E, Velasco-Ocana M, Marcos S. Full 3-D OCT-based pseudophakic custom computer eye model. Biomed Opt Express. 2016;7(3):1074–88.
61. Rosales P, Marcos S. Customized computer models of eyes with intraocular lenses. Opt Express. 2007;15(5):2204–18.
62. Tabernero J, Piers P, Benito A, Redondo M, Artal P. Predicting the optical performance of eyes implanted with IOLs to correct spherical aberration. Invest Ophthalmol Vis Sci. 2006;47(10):4651–8.
63. Hoffmann PC, Lindemann CR. Intraocular lens calculation for aspheric intraocular lenses. J Cataract Refract Surg. 2013;39(6):867–72.
64. Norrby S. Sources of error in intraocular lens power calculation. J Cataract Refract Surg. 2008;34:368–76.
65. Ortiz S, Perez-Merino P, Gambra E, de Castro A, Marcos S. In vivo human crystalline lens topography. Biomed Opt Express. 2012;3:2471–88.
66. Pérez-Merino P, Velasco-Ocana M, Martinez-Enriquez E, Marcos S. OCT-based crystalline lens topography in accommodating eyes. Biomed Opt Express. 2015;6:5039–54.
67. Martinez-Enriquez E, Sun M, Velasco-Ocana M, Birkenfeld J, Pérez-Merino P, Marcos S. Optical coherence tomography based estimates of crystalline lens volume, equatorial diameter, and plane position. Invest Ophthalmol Vis Sci. 2016;57(9):OCT600–10.
68. Martinez-Enriquez E, Pérez-Merino P, Velasco-Ocana M, Marcos S. OCT-based full crystalline lens shape change during accommodation in vivo. Biomed Opt Express. 2017;8(2):918–33.
69. Martinez-Enriquez E, Pérez-Merino P, Durán-Poveda S, Jiménez-Alfaro I, Marcos S. Estimation of intraocular lens position from full crystalline lens geometry: towards a new generation of intraocular lens power calculation formulas. Sci Rep. 2018;8(1):9829.
70. Applegate RA, Ballentine C, Gross H, Sarver EJ, Sarver CA. Visual acuity as a function of Zernike mode and level of root mean square error. Optom Vis Sci. 2003;80(2):97–105.
71. Cheng X, Bradley A, Thibos LN. Predicting subjective judgment of best focus with objective image quality metrics. J Vis. 2004;4:310–21.
72. de Gracia P, Dorronsoro C, Gambra E, Marin G, Hernández M, Marcos S. Combining coma with astigmatism can improve retinal image over astigmatism alone. Vision Res. 2010;50(19):2008–14.
73. Alió JL, Peña-García P, Abdulla Guliyeva F, Soria FA, Zein G, Abu-Mustafa SK. MICS with toric intraocular lenses in keratoconus: outcomes and predictability analysis of postoperative refraction. Br J Ophthalmol. 2014;98(3):365–70.
74. Pérez-Merino P, Marcos S. Effect of intraocular lens decentration on image quality tested in a custom model eye. J Cataract Refract Surg. 2018;44(7):889–96.
75. Applegate RA, Marsack JD, Thibos LN. Metrics of retinal image quality predict visual performance in eyes with 20/17 or better visual acuity. Optom Vis Sci. 2006;83(9):635–40.
76. Cheng X, Bradley A, Hong X, Thibos L. Relationship between refractive error and monochromatic aberrations of the eye. Optom Vis Sci. 2003;80:43–9.
77. Cheng X, Thibos L, Bradley A. Estimating visual quality from wavefront aberration measurements. J Refract Surg. 2003;19:579–84.
78. Watson AB. Computing human optical point spread functions. J Vis. 2015;15(2):26.
79. Águila-Carrasco AJ, Read SA, Montés-Micó R, Iskander DR. The effect of aberrations on objectively assessed image quality and depth of focus. J Vis. 2017;17(2):2.
80. Iskander DR. Computational aspects of the visual Strehl ratio. Optom Vis Sci. 2006;83(1):57–9.